Protein *O*-fucosyltransferase 2–mediated *O*-glycosylation of the adhesin MIC2 is dispensable for *Toxoplasma gondii* tachyzoite infection

Received for publication, August 14, 2018, and in revised form, November 27, 2018 Published, Papers in Press, December 4, 2018, DOI 10.1074/jbc.RA118.005357

Sachin Khurana[‡§1], Michael J. Coffey[‡§1], Alan John[‡§], Alessandro D. Uboldi[‡§], My-Hang Huynh[¶], Rebecca J. Stewart[‡§], Vern B. Carruthers[¶], Christopher J. Tonkin[‡§2], Ethan D. Goddard-Borger[‡§3], and Nichollas E. Scott[‖4]

From the [‡]Walter and Eliza Hall Institute of Medical Research, Parkville, Victoria 3052, Australia, the [§]Department of Medical Biology, University of Melbourne, Parkville, Victoria 3010, Australia, the [¶]Department of Microbiology and Immunology, University of Michigan Medical School, Ann Arbor, Michigan 48109, and the [‖]Department of Microbiology and Immunology, University of Melbourne at the Peter Doherty Institute for Infection and Immunity, Parkville, Victoria 3010, Australia

Edited by Gerald W. Hart

***Toxoplasma gondii* is a ubiquitous, obligate intracellular eukaryotic parasite that causes congenital birth defects, disease in immunocompromised individuals, and blindness. Protein glycosylation plays an important role in the infectivity and evasion of immune responses of many eukaryotic parasites and is also of great relevance to vaccine design. Here we demonstrate that micronemal protein 2 (MIC2), a motility-associated adhesin of *T. gondii*, has highly glycosylated thrombospondin repeat (TSR) domains. Using affinity-purified MIC2 and MS/MS analysis along with enzymatic digestion assays, we observed that at least seven *C*-linked and three *O*-linked glycosylation sites exist within MIC2, with >95% occupancy at these *O*-glycosylation sites. We found that addition of *O*-glycans to MIC2 is mediated by a protein *O*-fucosyltransferase 2 homolog (TgPOFUT2) encoded by the *TGGT1_273550* gene. Even though POFUT2 homologs are important for stabilizing motility-associated adhesins and for host infection in other apicomplexan parasites, loss of TgPOFUT2 in *T. gondii* had only a modest impact on MIC2 levels and the wider parasite proteome. Consistent with this, both plaque formation and tachyzoite invasion were broadly similar in the presence or absence of TgPOFUT2. These findings indicate that TgPOFUT2 *O*-glycosylates MIC2 and that this glycan, in contrast to previous findings in another study, is dispensable in *T. gondii* tachyzoites and for *T. gondii* infectivity.**

This work was supported by National Health and Medical Research Council of Australia (NHMRC) Project Grant APP1100164 (to N. E. S.). The authors declare that they have no conflicts of interest with the contents of this article.

This article contains Figs. S1–S4 and Tables S1–S5.

The MS proteomics data were deposited in the ProteomeXchange Consortium via the PRIDE partner repository with the dataset identifiers PXD010714 and PXD011440.

[1] Both authors contributed equally to this work.

[2] Recipient of Australian Research Council (ARC) Future Fellowship FT120100164, which supported this work. To whom correspondence may be addressed: E-mail: tonkin@wehi.edu.au.

[3] To whom correspondence may be addressed: E-mail: goddard-borger.e@wehi.edu.au.

[4] Supported by Overseas (Biomedical) Fellowship APP1037373 and a University of Melbourne Early Career Researcher Grant Scheme (proposal 603107). To whom correspondence may be addressed: E-mail: nichollas.scott@unimelb.edu.au.

The phylum Apicomplexa is comprised of a large group of obligate intracellular eukaryotic parasites, many of which have medical and agricultural significance. Pathogenic apicomplexan species include *Plasmodium* spp. (malaria), *Cryptosporidium* spp. (cryptosporidiosis), *Theileria* spp. (theileriosis), *Babesia* spp. (babesiosis), and the most ubiquitous of all, *Toxoplasma gondii* (toxoplasmosis). *T. gondii* infects 30–80% of the human population, and, although largely self-limiting in healthy individuals, it can cause major problems in the immunosuppressed and lead to congenital birth defects when contracted while pregnant (1). Some countries have extremely high rates of progressive blindness caused by toxoplasmic retinopathy, which has no curative treatment (1–3).

All apicomplexan parasites must migrate through host tissues and invade cells to survive and to cause disease; thus, this process is considered an excellent therapeutic target. Central to dissemination and invasion is a unique form of cellular locomotion termed "gliding motility." Gliding motility requires the apical release of transmembrane adhesins from microneme organelles onto the parasite surface (4), which provides an anchor to the extracellular environment and/or host cells. The current model posits that motility is initiated when an actomyosin-based "glideosome," which lies just underneath the plasma membrane, binds to the cytoplasmic tails of adhesins and drags them to the rear of the parasite, exerting a forward-acting force, thus driving forward motion (5–7).

Motility-associated adhesins in Apicomplexa vary between species and differ in expression across the various life cycle stages, reflecting the diversity of host cells that are targeted by this group of parasites. For example, *Plasmodium* spp. use a range of adhesins that specifically bind to erythrocyte receptors in asexual blood stages and other adhesins in stages that infect mosquitoes or the human liver (8, 9). Although little is known about the host cell receptors of *T. gondii*, a diverse array of putative adhesins is contained within their micronemes, which goes some way toward explaining the remarkably diverse range of host species and cell types that can be infected by this zoonotic parasite. Common features exist among these motility and invasion-associated adhesin proteins, including the recur-

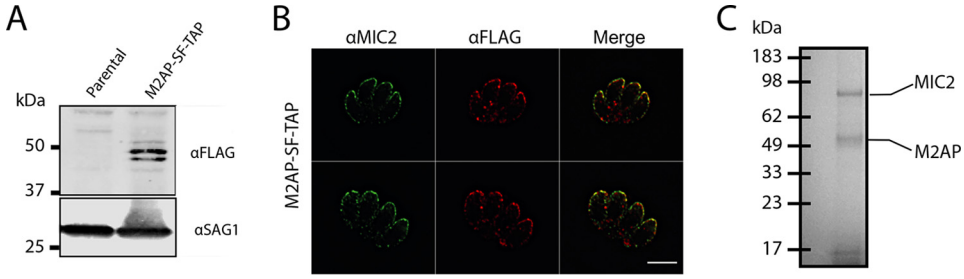

Figure 1. Establishment and validation of the M2AP SF-TAP *T. gondii* line. *A*, addition of a C-terminally appended SF-TAP tag enables detection of M2AP within the *T. gondii* line M2AP SF-TAP compared with the parental line. *B*, M2AP, detected using α-FLAG, co-localizes with MIC2 within intracellular tachyzoites. *Scale bar* corresponds to 5 μm. *C*, enrichment of M2AP SF-TAP tagged protein enables the isolation of the MIC2-M2AP complex to high purity, as determined by Coomassie-stained gels (image reproduced from Fig. 4*C*).

rence of one or more thrombospondin repeat (TSR)[5] domains (10).

Apicomplexan TSR-containing adhesin proteins are the only examples of TSRs found outside metazoa, but their function in mediating infection remains poorly understood. Metazoan TSRs are glycosylated in the endoplasmic reticulum with the *O*-linked glycan α-D-glucopyranosyl-1,3-β-L-fucopyranoside (GlcFuc) and *C*-linked α-D-mannopyranosides (*C*-Man) (11). Protein *O*-fucosyltransferase 2 (POFUT2) initiates metazoan TSR *O*-glycosylation and plays an important role in the folding and stabilization of these proteins (12–16). Recently, TSR *O*-glycosylation has also been observed in *Plasmodium falciparum* and *Plasmodium vivax* (17, 18); this *O*-glycan is initiated by a homolog of POFUT2 and is important for stabilizing proteins with TSR domains and efficient host infection (19). *O*-glycosylation of TSR domains may also be an important consideration in vaccine design (20).

Endogenous TSR *O*-glycosylation has yet to be observed in *T. gondii*; however, it does encode a putative POFUT2 (TGGT1_273550), and recombinant expression of *T. gondii* proteins in Chinese hamster ovary cells results in modification of parasite protein with the GlcFuc and *C*-Man glycans (21). Here we generate a *T. gondii* line to facilitate bulk purification of micronemal protein 2 (MIC2) directly from tachyzoites to map endogenous glycosylation sites on this motility-associated adhesin that possesses six TSR domains. We go on to demonstrate that a *T. gondii* POFUT2 is encoded by TGGT1_273550 and that loss of *O*-glycosylation has only a modest impact on MIC2 levels, the wider tachyzoite proteome, and infectivity.

Results

MIC2 is glycosylated at multiple sites to high occupancy

To explore the glycosylation of MIC2, we generated a *T. gondii* line in which the MIC2 associated protein (M2AP) possessed a C-terminal strep-FLAG tandem affinity purification (SF-TAP) tag to allow convenient purification of the M2AP–MIC2 complex. Western blotting using FLAG antibodies confirmed that M2AP was tagged (Fig. 1*A*). Further, we showed, using immunofluorescence, that M2AP–SF-TAP largely co-localizes with MIC2, as expected (Fig. 1*B*). The SF-TAP–tagged M2AP enabled simple high-yielding batch purification of the M2AP–MIC2 complex from bulk tachyzoite cultures (Fig. 1*C*). We then identified glycosylation events using MS/MS analysis in combination with multiple enzymatic digestions approaches. Enzymatic digestions comprised of trypsin, gluC, and sequential gluC and then trypsin, which was analyzed using higher-energy collision dissociation (HCD) and electron transfer and higher-energy collision dissociation (EThcD) fragmentation approaches (Ref. 22 and Table S1). Using these approaches, we detected multiple *C*-glycosylation and *O*-glycosylation events in five of the six TSR domains of MIC2 (Fig. 2, *A* and *B*, and Fig. S1). Within these TSR domains a total of five previously unreported *C*-glycosylation events were observed (Fig. 2*B*), corresponding to Trp^{276}, Trp^{279}, Trp^{348}, Trp^{351}, and Trp^{479}, all lying within the *C*-mannosyltransferase consensus motifs (W*XX*W/C (23)). Because of the stable nature of *C*-glycosylation, these sites were readily assigned with rich fragmentation around Trp residues, enabling confident identification. Electron transfer–based fragmentation was used to localize the labile *O*-glycosylation events to three sites within MIC2: Ser^{285} (Fig. 3*A*), Ser^{485} (Fig. 3*B*), and Thr^{546} (Fig. 3, *C* and *D*). Using EThcD, fragmentation ions decorated with and without GlcFuc were observed (Fig. 3, *A* and *D*), both supporting the presence of the labile GlcFuc modification and the sites of modification. An additional *O*-glycosylation event was also observed within TSR2 on the semitryptic peptide ^{346}GEWSAWSASCGNATR^{360}, but the exact site of modification was unable to be precisely assigned (Table S1). We compared the abundance of unmodified and modified peptides covering these sites to better understand *O*-glycan occupancy (Table S2), and all of the *O*-glycosylated peptides were found to be the dominant observable species (Fig. 3, *E–G*). To summarize, MIC2 is endogenously modified with at least four *O*-glycans (GlcFuc) and seven *C*-glycans (*C*-Man) (Figs. 2 and 3) within TSR1, 2, 4, and 5, with the *O*-glycan occupancy greater than 95% for sites Ser^{285}, Ser^{485}, and Thr^{546}.

TGGT1_273550 encodes the T. gondii POFUT2

We were interested in determining the enzyme responsible for deposition of *O*-glycans on MIC2. A BLAST search of the *T. gondii* GT1 genome using *Homo sapiens* POFUT2

[5] The abbreviations used are: TSR, thrombospondin repeat; GlcFuc, β-D-glucopyranosyl-1,3-α-L-fucopyranoside; *C*-Man, *C*-linked α-D-mannopyranoside; SF-TAP, strep-FLAG tandem affinity purification; HCD, higher-energy collision dissociation; EThcD, electron transfer and higher-energy collision dissociation; HA, hemagglutinin; LFQ, label-free quantitative; HFF, human foreskin fibroblast; TRAP, thrombospondin repeat anonymous protein, IFA, immunofluorescence assay; LIC, ligation-independent cloning; DME, Dulbecco's Modified Eagle's Medium; AGC, automatic gain control.

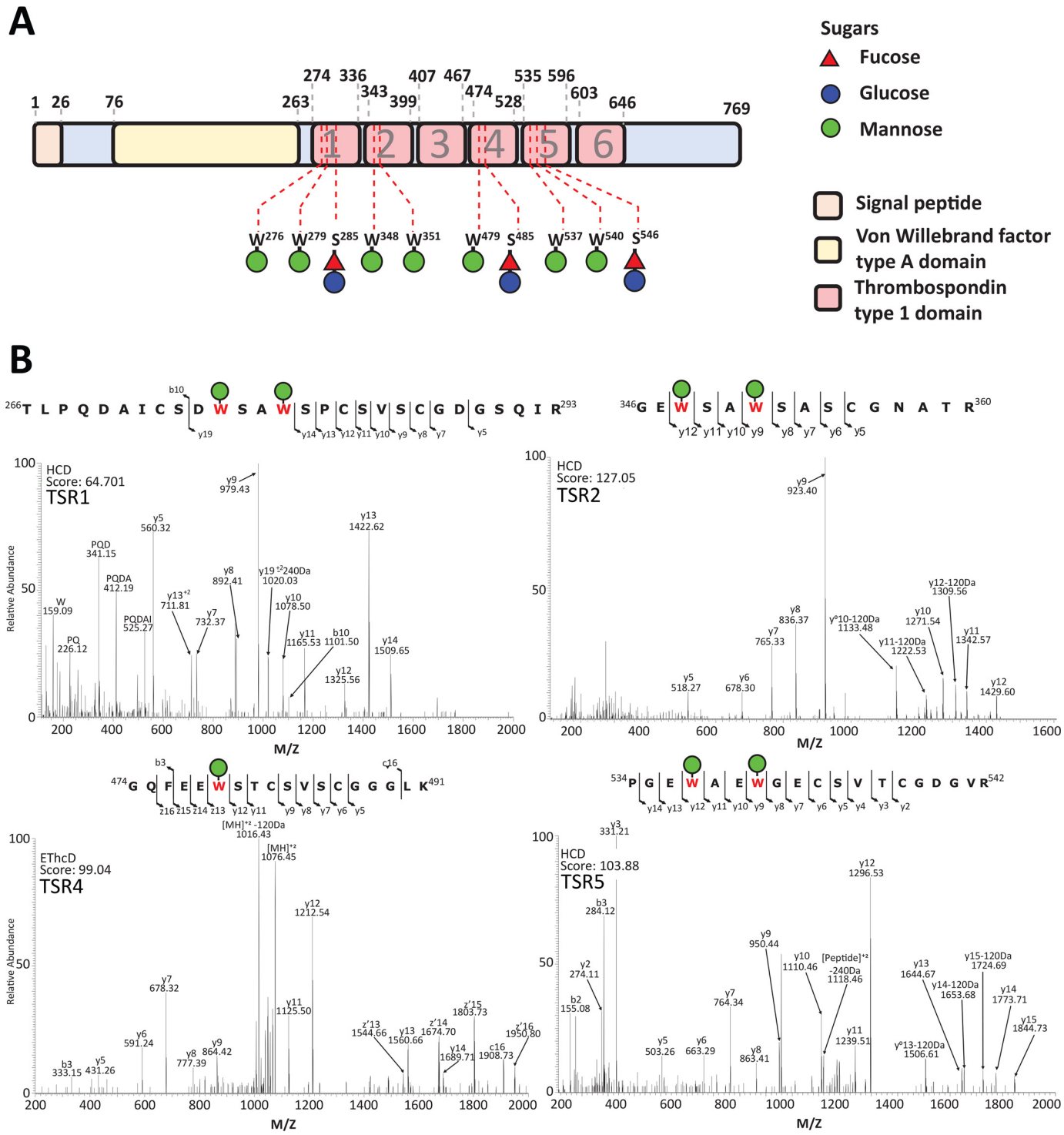

Figure 2. Characterization of MIC2 glycosylation events. *A*, within MIC2, ten glycosylation sites were identified, corresponding to seven *C*-glycosylation events and three GlcFuc sites of modification. The residues modified and the corresponding carbohydrate modification are mapped to the MIC2 sequence. All observed glycosylation events lie within the TSR domains. *B*, peptides containing observed the *C*-glycosylation events Trp^{276}, Trp^{279}, Trp^{348}, Trp^{351}, Trp^{479}, Trp^{537} and Trp^{540}.

(CAC24557.1 (24)) as the query sequence suggested that the protein encoded by TGGT1_273550 was most likely the *T. gondii* POFUT2 homolog. To investigate the function of TgPOFUT2, we first introduced a C-terminal triple HA (HA_3) epitope tag using single cross-over recombination (Fig. 4*A*). To ensure that HA tagging did not interfere with function, we also monitored MIC2 glycosylation in TgPOFUT2-HA and could show that this was indistinguishable from the parent M2AP-SF line (Fig. S3). This then allowed us to monitor disruption of TgPOFUT2 using CRISPR/Cas9-based gene knockout (Fig. 4*A* and Fig. S2, *A* and *B*), which was all performed in the M2AP–SF-TAP genetic background to provide a convenient means to purify and analyze MIC2 in the absence of TgPOFUT2 (Δ*tgpofut2*). We first looked to see whether loss of TgPOFUT2

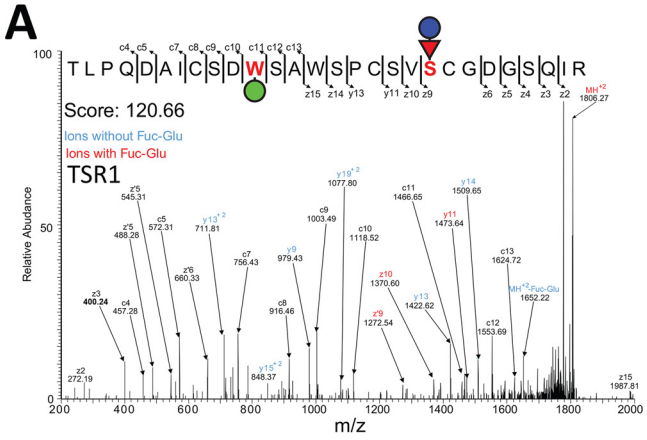
A
T L P Q D A I C S D W S A W S P C S V S C G D G S Q I R
Score: 120.66
Ions without Fuc-Glu
Ions with Fuc-Glu
TSR1
Relative Abundance
m/z

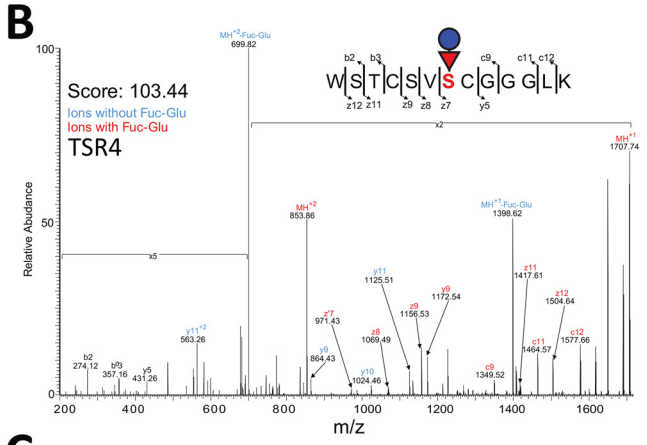
B
W S T C S V S C G G G L K
Score: 103.44
Ions without Fuc-Glu
Ions with Fuc-Glu
TSR4
Relative Abundance
m/z

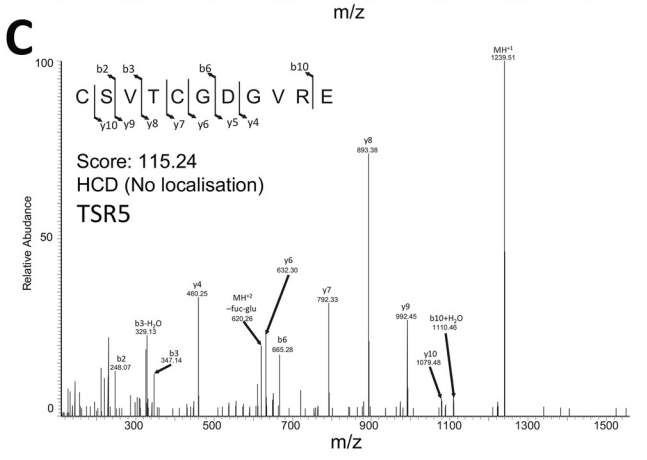
C
C S V T C G D G V R E
Score: 115.24
HCD (No localisation)
TSR5
Relative Abundance
m/z

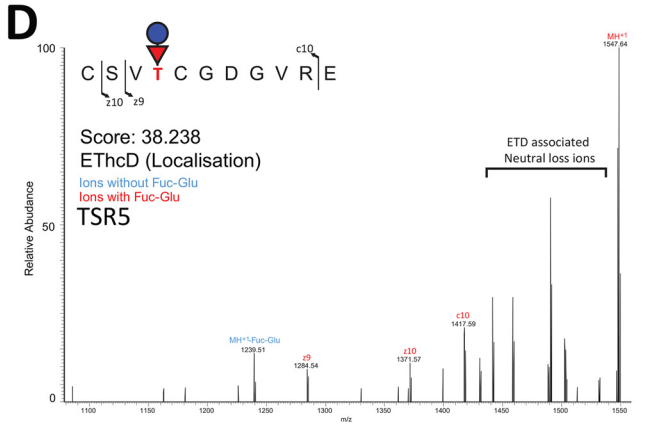
D
C S V T C G D G V R E
Score: 38.238
EThcD (Localisation)
Ions without Fuc-Glu
Ions with Fuc-Glu
TSR5
ETD associated
Neutral loss ions
Relative Abundance

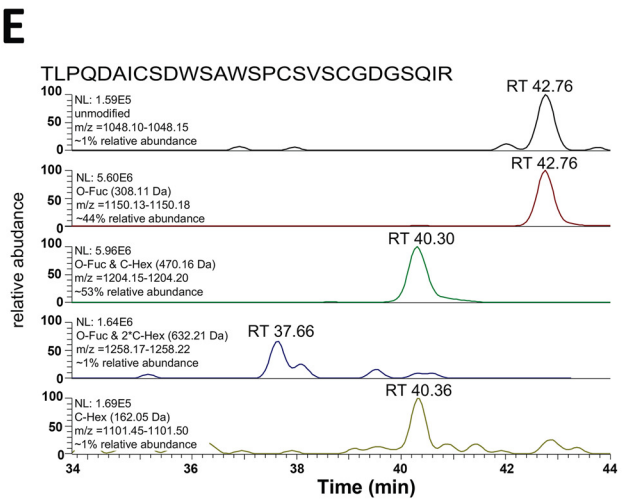
E
TLPQDAICSDWSAWSPCSVSCGDGSQIR
RT 42.76
RT 42.76
RT 40.30
RT 37.66
RT 40.36
relative abudance
Time (min)

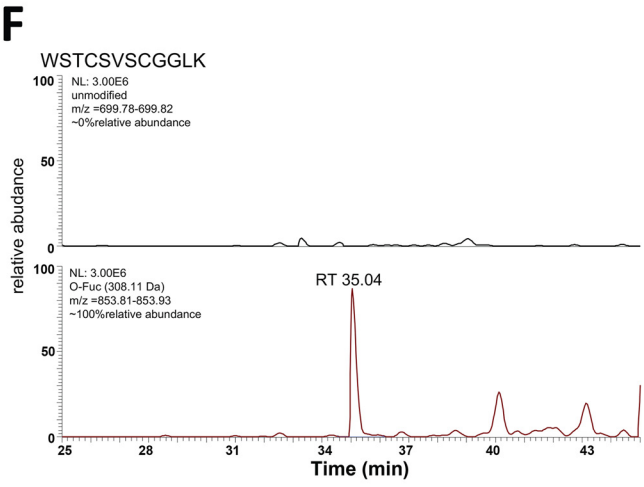
F
WSTCSVSCGGLK
RT 35.04
relative abudance
Time (min)

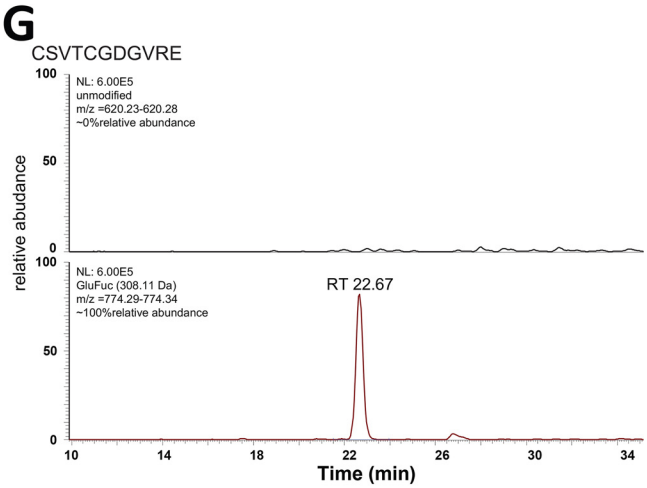
G
CSVTCGDGVRE
RT 22.67
relative abudance
Time (min)

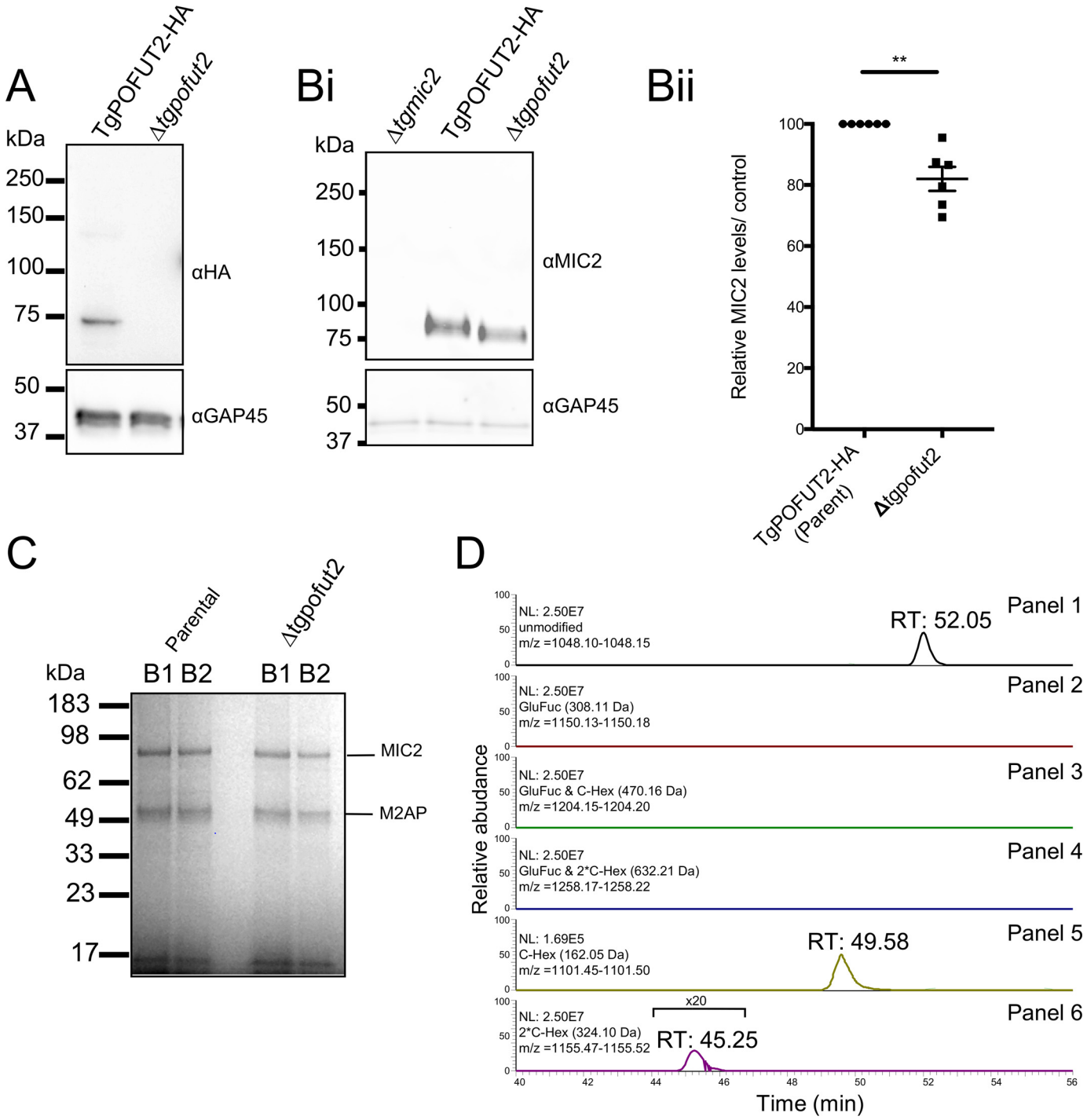

Figure 4. TGGT1_273550 encodes *T. gondii* POFUT2. *A*, endogenously tagging TgPOFUT2 with HA enabled detection in tachyzoites. This band is absent in a Δ*tgpofut2* line. *B*, loss of POFUT2 leads to a change in the migration of MIC2 and a small, ~20% decrease in MIC2. Data points refer to individual biological replicates, showing mean ± S.E. *p* values were calculated using a paired *t* test; **, $p < 0.01$. *C*, Coomassie-stained gel of isolation of M2AP enables co-isolation of MIC2 in the Δ*tgpofut2* line at comparable levels, with *B1* and *B2* corresponding to two independent isolations from biological replicates. *D*, for the peptide ^{266}TLPQDAICSDWSAWSPCSVSCGDGSQIR^{293}, unmodified, single, and doubled C-glycosylated peptides from MIC2 were identified, but no GlcFuc-containing species were observed. Extracted ion chromatograms demonstrate that these identified forms are clearly detectible in *panels 1*, *5*, and *6*, whereas even at the MS1 level, no ions corresponding to the GlcFuc glycoforms were observed in *panels 2–4*.

Figure 3. Sites of *O*-fucosylations of MIC2 are modified at a high occupancy. *A*, analysis of tryptic digested MIC2 with EThcD fragmentation enabled identification of the *C*-glycosylated and GlcFuc within ^{266}TLPQDAICSDWSAWSPCSVSCGDGSQIR^{293}, with the site of GlcFuc localized to S^{285}. *B*, analysis of trypsin- and GluC-digested MIC2 with EThcD fragmentation enabled identification of glycosylated ^{479}WSTCSVSCGGGLK^{491}, with the site of GlcFuc localized to Ser^{485}. Analysis of GluC-digested MIC2 using a combination of HCD (*C*) and EThcD (*D*) fragmentation enabled localization of GlcFuc to Thr^{546} on the glycopeptide ^{543}CSVTCGDGVRE^{553}. The GlcFuc-containing glycoforms of these peptides were the most abundant forms observed (*E–G*), supporting the hypothesis that these sites are occupied at high occupancy.

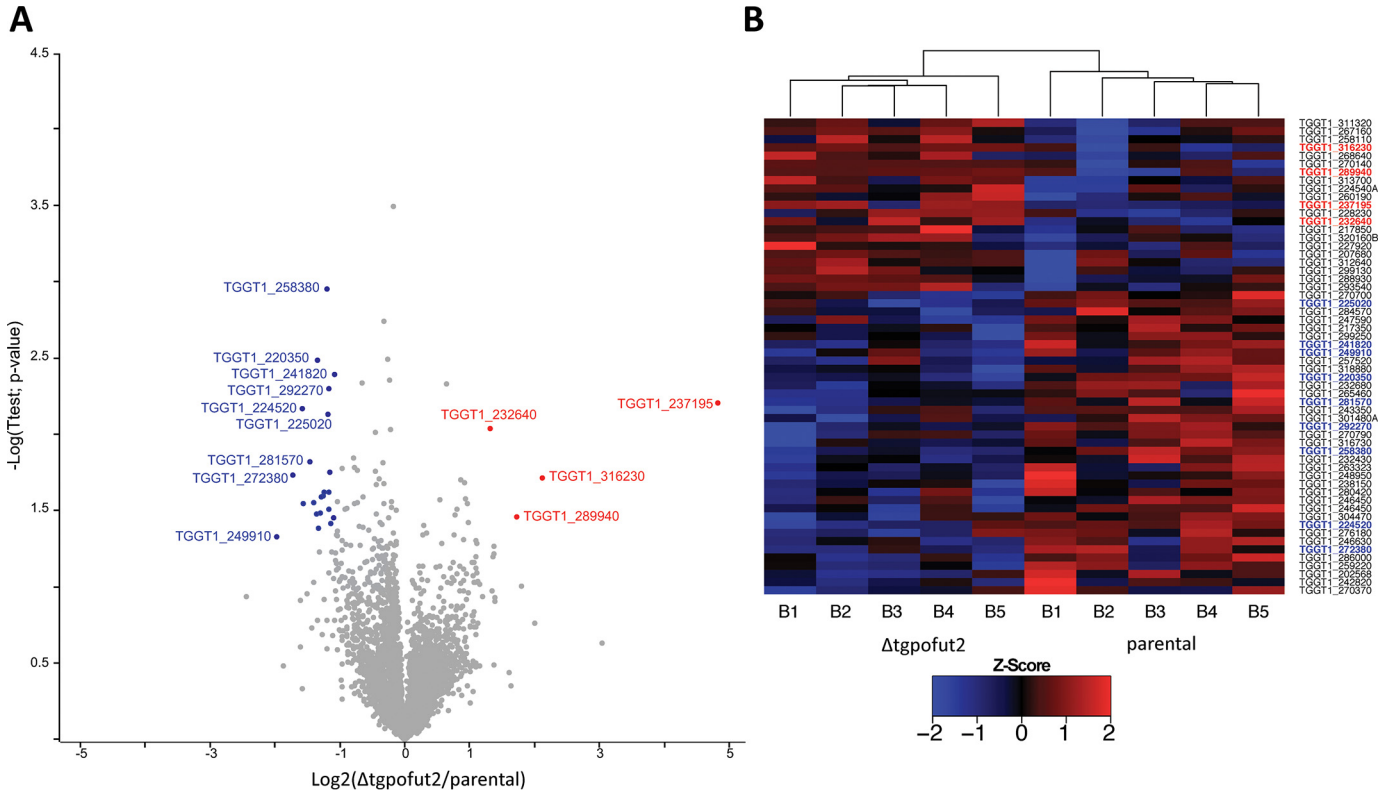

Figure 5. Quantitative proteomic analysis of Δ*tgpofut2* compared with the parental line. Label-free quantification of isolated tachyzoites was undertaken to compare Δ*tgpofut2* with the parental line. *A*, identified proteins are presented as a volcano plot depicting mean LFQ intensity ratios of Δ*tgpofut2 versus* the parental line plotted against logarithmic *t* test *p* values from five biological experiments of each line. *B*, heat map of z-scored values of the proteins observed to change between the Δ*tgpofut2* and the parental line, demonstrating the consistency of these changes across experiments.

impacted MIC2 protein levels, as observed for thrombospondin repeat anonymous protein (TRAP) in *P. falciparum* (19). Using quantitative western blots, we found only a small but consistent reduction in abundance compared with parental lines (Fig. 4*B*, *i* and *ii*). Interestingly, we also observed reproducible faster migration of MIC2 by SDS-PAGE, perhaps reflecting the small mass change and/or an increase in polypeptide hydrophobicity that results from loss of multiple *O*-glycans (Fig. 4*B*, *i*). We then used the SF-TAP handle to purify the MIC2–M2AP complex from both parental and Δ*tgpofut2* lines as before (Fig. 4*C*) and subjected these samples to trypsin digestion followed by MS analysis. In doing so, we could observe no difference in the ability of M2AP to precipitate MIC2, as observed by peptide abundance between both components, suggesting no difference in interaction between these two proteins. Monitoring the MIC2 glycopeptide ^{266}TLPQDAICSDWSAWSPCSVSCGDGSQIR^{293}, which can be both *C*- and *O*-glycosylated, provided insights into glycosylation changes within the Δ*tgpofut2* line (Fig. 4*D*, *panels 2–4*). We could not observe any GlcFuc-containing forms of this peptide, but we were readily able to identify the unmodified form of this peptide (retention time, 53.06 min) and both the singly and doubly *C*-glycosylated forms of this peptide (retention time, 49.58 and 45.25 min, respectively) (Fig. 4*D*, *panels 5* and *6*, Tables S3 and S4). Collectively, these data suggests that the *T. gondii* POFUT2 is encoded by TGGT1_273550 and that TSR *O*-glycosylation plays only a minor role in regulating MIC2 abundance.

Disruption of TgPOFUT2 results in modest alterations across the proteome

Because glycosylation systems can target multiple protein substrates, and because this modification is a known stabilizing factor, we hypothesized that the loss of TgPOFUT2 might disrupt a range of proteins beyond MIC2 (25, 26). To gain a better understanding of underlying changes that result from the loss of *O*-glycosylation in *T. gondii*, we conducted a global proteomics analysis comparing the parental strain with Δ*tgpofut2* using label-free quantitative (LFQ) proteomics (Table S5) (27). A total of 3839 unique *T. gondii* proteins were identified across biological replicates, with >3000 quantified proteins within each of the five parental and Δ*tgpofut2* replicates. We observed only modest changes in the proteome in response to the loss of TgPOFUT2 (Fig. 5*A*). These modest changes are reflected in the Pearson correlation (>0.95) observed between samples (Fig. S4). Using conventional thresholds (fold change more than ±1-fold and p >0.05), we observed a total of 26 proteins that decreased in abundance, whereas four increased in abundance within Δ*tgpofut2* compared with the parent (Fig. 5*A*). Even with less stringent thresholds (fold change more than ±1-fold and p >0.075), few additional alterations are observed across the proteome of the Δ*tgpofut2* strain (Fig. 5*B*, 37 decreasing and 21 increasing respectively). Although modest, these alterations are consistent across biological replicates (Fig. 5*B*) and suggest that loss of TSR *O*-glycosylation leads to small but real changes in the *T. gondii* proteome. Importantly, no TSR-containing pro-

teins were observed to undergo significant changes in abundance in response to loss of TgPOFUT2.

TSR O-glycosylation is not important for lytic stage growth, MIC2 trafficking, or host cell invasion

We furthered our phenotypic analysis to reveal whether TgPOFUT2 contributes to lytic stage growth in relation to what is known about MIC2 in *T. gondii*. To do this, we first performed plaque assays where parental and Δ*tgpofut2* parasites were left to grow on human foreskin fibroblast (HFF) monolayers over 7–8 days, and then zones of lysis (plaques) were quantitated by size and number. Here we confirmed, as described previously, that parasites lacking MIC2 cause a reduction in plaque size compared with the parental line (Fig. 6*A*) (28–30). Δ*tgpofut2* tachyzoites, on the other hand, had mildly smaller plaques than the parental TgPOFUT2-HA line, but not nearly as severe as complete loss of MIC2 (Fig. 6*A*, *i* and *ii*), which is consistent with the mild CRISPR fitness score (-0.34 $\log_2$). We could not detect any significant difference in host cell attachment of Δ*tgpofut2* compared with the dramatic defect upon complete loss of MIC2 (Fig. 6*A*, *iii*).

Posttranslational modifications can affect protein trafficking, and we therefore assessed the localization of M2AP and MIC2 in Δ*tgpofut2* by IFA. Here we could observe no difference in localization of either MIC2 or M2AP, suggesting that *O*-glycosylation plays no detectable role in protein trafficking (Fig. 6*B*). We also specifically monitored for defects in host cell invasion after 2-, 10-, and 30-min incubation on HFFs (Fig. 6*C*). Again, we could see no difference in invasion capacity at any time point when using this assay, suggesting that TgPOFUT2 is not important for MIC2 function *in vitro*.

Discussion

The recent recognition of the importance of glycosylation at the host–pathogen interface in parasites such as *P. falciparum* (19) and *Trypanosoma brucei* (31) has demonstrated the need to better understand glycosylation within phylogenetically distinct eukaryotic parasites. Here we demonstrate that *T. gondii,* the causative agent of toxoplasmosis, has a functional POFUT2 homologue that is responsible for initiating *O*-glycosylation of TSR domains on MIC2. We confirm that at least three sites in MIC2 (Ser^{285}, Ser^{485}, and Thr^{546}; Fig. 3) are modified by GlcFuc in addition to seven sites of *C*-glycosylation. These *O*-glycosylation sites lie within the previously proposed POFUT2 consensus sequon C*XX*(S/T)C (11, 24, 32) and suggest that TgPOFUT2 has a similar substrate preference as metazoan POFUT2 enzymes. Our data demonstrates that these sites are modified to a high occupancy, with few peptide species lacking the *O*-glycans observed in parental MIC2 preparations. The loss of *O*-glycans in the Δ*tgpofut2* line did not appear to impact *C*-glycosylation, as previously observed sites were readily detected within Δ*tgpofut2*, suggesting that, in *T. gondii* MIC2, these two modifications operate independently of each other.

Previous work on mammalian POFUT2 has revealed that *O*-glycosylation is essential for mice with homozygous disruption of POFUT2 being embryonic lethal after implantation (15). In humans, loss of *O*-glycan elongation because of mutation in the β-1,3-glucosyltransferase (B3GLCT) (33, 34) leads to Peter plus syndrome (35). These defects are driven by the requirement for the complete GlcFuc disaccharide for endoplasmic reticulum quality control, where this glycan influences the folding and stability of proteins with TSR domains (36, 37). Similarly, we have observed that loss of *O*-fucosylation in *P. falciparum* sporozoites leads to destabilization of the key adhesin TRAP (19, 38). However, within *T. gondii*, loss of TgPOFUT2 appears not to be the case. We show that loss of TgPOFUT2 only leads to a small change in MIC2 levels and has no detectable difference in its ability to bind to its accessory protein M2AP or affect its protein trafficking. The small change in MIC2 levels is accompanied by a modest reduction (~20%) in plaque size, which is consistent with the recent CRISPR-based fitness score assigned by Sidik *et al.* (39) to TgPOFUT2 (-0.34 $\log_2$), which, compared with loss of MIC2 (-1.17 $\log_2$), is very mild. However, we cannot discount that TgPOFUT2 may be more important for *in vivo* (mouse) infection models, where optimal tissue dissemination and invasion are critical for parasite survival. It may also be that TgPOFUT2 plays an important role in other stages of the parasite's lifecycle (*e.g.* bradyzoites and enteric feline stages), which was not assessed in this study. Indeed, the *P. falciparum* POFUT2 ortholog does not appear to have a detectable role in blood stages but does during transmissible stages (19).

Consistent with the nonessential nature of TgPOFUT2 in tachyzoites, we observed few changes across the proteome (Fig. 4). The changes we observed were modest in magnitude but consistent across replicates, suggesting that TgPOFUT2 targets a limited repertoire of substrates, in line with other POFUT2 enzymes (24, 32). Interestingly, the absence of any dramatic decreases in abundance suggests that few proteins undergo destabilization, as observed with TRAP in *P. falciparum* (19). A number of proteins were observed to decreased within Δ*tgpofut2*, which may contribute to the observed phenotypes, including TGGT1_270700, now known as *MYR2*, which was recently shown to be essential for effector translocation into the host cell (40). We did not assess effector translocation in this study, and therefore this is worthy of more attention in the future. Additionally, we note that multiple members of the glycosylphosphatidylinositol-anchored SRS superfamily (41) are altered in response to Δ*tgpofut2*, with an observed decrease in TGGT1_292270 (SRS36C) and an increase in TGGT1_292280 (SRS36D). As these surface antigens have been shown to modulate multiple aspects of infection (42), the function of these proteins may be worth following up. Surprisingly the most profound change we observed within the proteome of Δ*tgpofut2* was an increase in the hypothetical protein TGGT1_237195. This protein is not associated with *T. gondii* parasite fitness *in vitro* (39), and it has yet to be characterized how or why the loss of Δ*tgpofut2* results in an increase in abundance. It is important to note that none of these proteins contain the TgPOFUT2 C*XX*(S/T)C sequon, suggesting that they are not direct targets of TgPOFUT2 but may be influenced indirectly by the loss of *O*-fucosylation. We did not see any difference in MIC2 levels in our global proteome analysis as we saw with quantitate Western blotting, suggesting that this technique may not be sensitive enough to detect milder changes in protein levels.

The fact that TSR *O*-glycosylation does not appear to be important for the stability or trafficking of MIC2, in contrast to

observations from TRAP in *P. falciparum* (19), may be due to the intimate association of MIC2 and M2AP. M2AP contributes to trafficking of this important adhesin to the micronemes and assists with its function (43, 44). Other coccidian parasites, including *Neospora caninum* and *Eimeria tenella* also express orthologs of *T. gondii* M2AP (45, 46). However, TRAP and

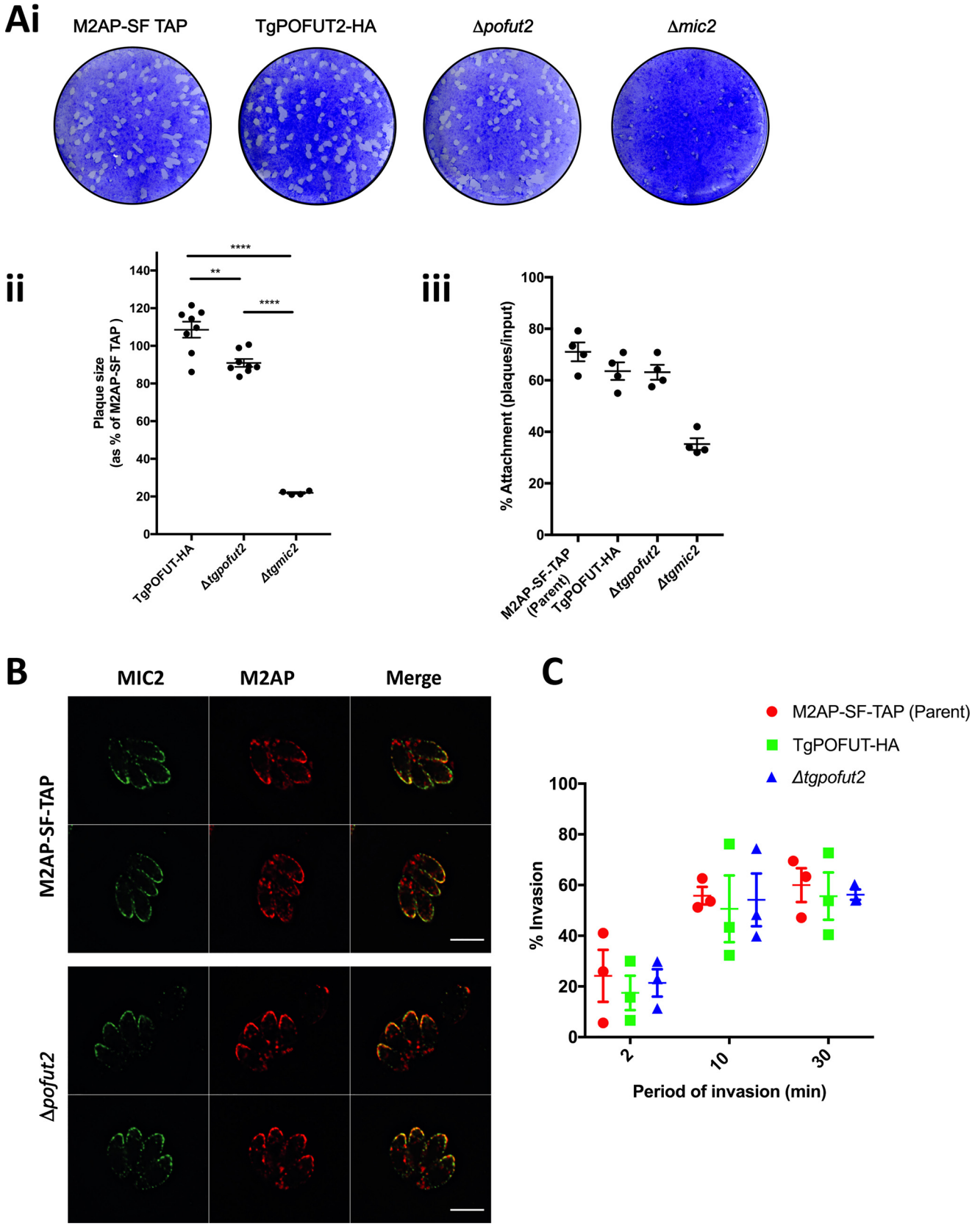

related proteins in *P. falciparum* are not known to associate with an analogous protein, and therefore it is plausible that this makes *O*-glycosylation more important for protein folding and trafficking in these species. We have also shown here that MIC2 is heavily *C*-mannosylated, which alludes to the possibility that this modification could be important for the function of MIC2. This possibility is reflected by the fitness score assigned by Sidik *et al.* 39 to the putative *C*-mannosyltransferase in *T. gondii* (TGGT1_280400, -2.37 $\log_2$), which is suggestive of severe defects in tachyzoite function, although this remains to be further investigated.

During compilation of this manuscript, we were made aware of another body of work that also functionally characterizes POFUT2 in *T. gondii*. Bandini *et al.* (62) largely come to the same conclusion as reported here, including identification of similar glycosylation sites and demonstrating that TgPOFUT2 is responsible for their deposition. Further, Bandini *et al.* (62) also demonstrate that loss of TgPOFUT2 results in an apparent mild decrease in MIC2 levels (although they do not quantify this). Their study does diverge from this one in concluding that Δ*tgpofut2* has a defect in host cell attachment and invasion, which appears to be similar to complete loss of MIC2. From careful comparison of experimental protocols, the only difference we have identified is the method by which invasion assays were performed. We used $[K^+]$ shift to promote synchronous invasion whereas the Bandini *et al.* study (62) did not. $[K^+]$ shift strongly promotes cytosolic Ca^{2+} signaling and microneme secretion, resulting in synchronous motility and invasion (47, 48). It could be that these differences in conditions are enough to subtly effect invasion efficiency and thus explain the differences in the two studies. However, it is important to note that if, indeed, Δ*tgpofut2* has an invasion defect, then this would be the first mutant to do so without having an appreciable change in plaquing capacity. Regardless, dissecting out the reasons for the differences between the two studies might reveal novel and interesting biology regarding the role of fucosylation in MIC2 and invasion biology more generally.

In summary, TgPOFUT2 is responsible for *O*-glycosylation of TSR domains in MIC2. Loss of this modification leads to only small changes in MIC2 abundance, in contrast to the fate of TRAP in *P. falciparum* (19) and little to no impact on parasite invasiveness *in vitro*. Loss of TgPOFUT2 also provides no profound changes in the tachyzoite proteome. Taken together, this demonstrates that TgPOFUT2 is dispensable for replication of *T. gondii* tachyzoites.

Materials and methods

Plasmid construction and transfection

The 3′ portion of the *tgm2ap* (TGGT1_214940) ORF was PCR-amplified using the primers 5′-TACTTCCAATCCAATTTAATGCTGCTTGAGCCGTGACAACAGATTAC-3′ and 5′-TCCTCCACTTCCAATTTTAGCCGCCTCATCGTCACTCGGCAGACGGC-3′ and LIC cloned into vector pSF-TAP.LIC.DHFR-TS as described previously (49). The pM2AP.SF-TAP construct was linearized within the *tgm2ap* homology region with PflMI prior to transfection into RHΔku80:HXGPRT tachyzoites (49). The 3′ portion of the *tgpofut2* (TGGT1_273550) ORF was PCR-amplified using the following primers: 5′-TAGTAGATCTAGCGATTAGCACTTTTTGG-3′ and 5′-AGCCCTAGGCAGTGTCGAACTGGGGTC-3′ and ligated into the BglII/AvrII sites of pgCH (Gra 1 5′-CAT-BglII/AvrII 3xHA). The pgCH-POFUT2–3xHA construct was linearized within the tgpofut2 homology region with MfeI prior to transfection into RHΔku80:HXG tachyzoites (49). This construct was linearized with Mfe1 (New England Biolabs) prior to transfection.

Tgpofut2 was knocked out using a unique guide selected by EuPaGDT (http://grna.ctegd.uga.edu/batch_tagging.html;[6] 61) combined with a homologous repair template containing the BLE cassette. The CRISPR target plasmid (50) was constructed by Q5 mutagenesis (New England Biolabs) with the common reverse primer 5′-AACTTGACATCCCCATTTAC-3′ (51) and the forward primer 5′-GAGACGGTAAGAACTGAGACGGTTTTAGAGCTAGAAATAGCAAG-3′. The BLE cassette was then amplified using Primestar Max (Takara) containing homologous flanking regions on either side of the Cas9 cut site with primers 5′-TGTCTGCTCAACCACCGTCGCTTGCTGTTAGGCCTCGTCGTCTAGAAGGTGGATGCGGGA-3′ and 5′-TGAATGGGAGACACGAGAGGAAGACGGTAAGAACTGAGCGATGTGGAGTCGTCTCAAGCG-3′. 10 μg of the Cas9 plasmid was combined with 20 μg of PCR product and then precipitated using ethanol/sodium acetate prior to transfection. The dried DNA was resuspended in 3 μl of elution buffer (Qiagen), followed by 20 μl pf P3 solution (Lonza). A washed parasite pellet containing $\sim 10^6$ tachyzoites was then resuspended in this solution and transfected using the code FI-115 in a 16-well nucleocuvette strip in an Amaxa 4D nucleofector (Lonza). Parasites containing the knockout construct were then selected as normal following addition of phleomycin and subsequently subcloned until a stable population was obtained. All transfections proceeded using either a Gene Pulser II (Bio-Rad) or an Amaxa 4D nucleofector (Lonza). Gene Pulser II transfection took place at 1.5 kV and 25 μF, as is standard with 15 μg of purified linearized DNA when seeking homologous integration.

Parasite culture

Transfection and *in vitro* culture *T. gondii* tachyzoites were cultured under standard conditions. Briefly, HFFs (ATCC SCRC-1041) were grown in Dulbecco's Modified Eagle's

[6] Please note that the JBC is not responsible for the long-term archiving and maintenance of this site or any other third party–hosted site.

Figure 6. Phenotypic analysis of Δ*tgpofut2* compared with the parental line. *A*, *i*, morphological assessment of plaque assays comparing the parental line (*TgM2AP-SF TAP*), *TgPOFUT2-HA*, Δ*tgpofut2* and Δ*mic2*). *ii*, numerical assessment of plaque size compared with the TgM2AP-SF TAP parental line and Δ*mic2*. *iii*, numerical assessment of plaque capacity, as a surrogate of host cell attachment, compared across all lines. *B*, IFA assessment of localization of MIC2, detected using αMIC2, and M2AP, detected using αFLAG, suggests that *O*-glycosylation plays no detectable role in protein trafficking. *Scale bars* correspond to 5 μm. *C*, invasion assays at 2, 10, and 30 min demonstrate no detectable difference in invasion capacity. Each data point represents the average value across a biological replicate and are collectively represented using mean ± S.E. *p* values were calculated using a one-way analysis of variance for *A*, *ii* and *iii*, and two-way analysis of variance for *C*; **, $p < 0.01$; ****, $p < 0.0001$.

Medium (DME) supplemented with 10% heat-inactivated cosmic calf serum (Hyclone) until confluency was reached. Upon *T. gondii* infection, HFFs with were refreshed with DME supplemented with 1% fetal calf serum. All cells were grown in humidified incubators at 37 °C/10% CO_2.

Purification of the M2AP–MIC2 complex

Parasites obtained from four T150 flasks confluent with HFFs were purified by filtration and collected by centrifugation (1000 × *g*, 10 min). The parasite pellet was washed once on ice with PBS (2 ml). The parasite pellet was resuspended in 1 ml of lysis buffer (50 mM Tris (pH 8), 150 mM NaCl, 1% Triton X-100, Roche Mini Protease Inhibitor Mixture, DNase) and lysed at room temperature for 20 min. The lysate was centrifuged (10,000 × *g*, 10 min, 4 °C) to remove cellular debris, and the supernatant was incubated with Streptactin II resin (200 μl of 50% slurry) at 4 °C for 1–2 h with nutation. The resin was collected in microspin columns (2000 × *g*, 2 min, 4 °C) and washed three times with 50 mM Tris (pH 8), 150 mM NaCl, 0.1% Triton X-100. The resin was then incubated with 2.5 mM desthiobiotin, 50 mM Tris (pH 8), 150 mM NaCl (200 μl per column, 20 min, 4 °C) and the eluate collected by centrifugation (2000 × *g*, 2 min, 4 °C) to provide the purified MIC2–M2AP complex.

Tryptic digest of gel-separated proteins

Affinity-purified MIC2–M2AP was separated using SDS-PAGE, fixed, and visualized with Coomassie G-250 according to the protocol of Kang *et al.* (52). Bands of interest were excised and destained in a 50:50 solution of 50 mM NH_4HCO_3/100% ethanol for 20 min at room temperature with shaking at 750 rpm. Destained samples were then washed with 100% ethanol, vacuum-dried for 20 min, and rehydrated in 50 mM NH_4HCO_3 plus 10 mM DTT. Reduction was carried out for 60 min at 56 °C with shaking. The reducing buffer was then removed, and the gel bands were washed twice in 100% ethanol for 10 min to remove residual DTT. Reduced ethanol-washed samples were sequentially alkylated with 55 mM iodoacetamide in 50 mM NH_4HCO_3 in the dark for 45 min at room temperature. Alkylated samples were then washed with two rounds of 100% ethanol and vacuum-dried. Alkylated samples were then rehydrated with 12 ng/μl trypsin (Promega) in 40 mM NH_4HCO_3 at 4 °C for 1 h. Excess trypsin was removed, gel pieces were covered in 40 mM NH_4HCO_3 and incubated overnight at 37 °C. Peptides were concentrated and desalted using C18 stage tips (53) before analysis by LC-MS.

In-solution Glu-C/trypsin digestion and double digestion

Affinity-purified MIC2–M2AP was resuspend in 50 μl of 20% trifluoroethanol and a diluted equal volume of reduction/alkylation buffer (40 mM tris(2-carboxyethyl)phosphine, 80 mM chloroacetamide, and 100 mM NH_4HCO_3). Samples were then heated at 40 °C for 30 min to aid denaturation and reduction/alkylation in the dark. Glu-C or trypsin was added (1/50 w/w) and allowed to incubate overnight at 37 °C. For double digestion after the initial Glu-C digestion, trypsin (1/50 w/w) was added and allowed to incubate overnight at 37 °C. Digested samples were acidified to a final concentration of 0.5% formic acid and desalted using C18 stage tips (53) before analysis by LC-MS.

Characterization of MIC2 using reverse-phase LC-MS

Purified peptides were resuspend in buffer A and separated using a two-column chromatography set up composed of a PepMap100 C18 20 mm × 75 μm trap and a PepMap C18 500 mm × 75 μm analytical column (Thermo Fisher Scientific). Samples were concentrated onto the trap column at 5 μl/min for 5 min and infused into an Orbitrap Fusion™ Lumos™ Tribrid™ mass spectrometer (Thermo Fisher Scientific) or Orbitrap™ Q-exactive™ HF (Thermo Fisher Scientific) at 300 nl/min via the analytical column using a Dionex Ultimate 3000 Ultra-Performance Liquid Chromatography (UPLC) instrument (Thermo Fisher Scientific). 75-min gradients were run, altering the buffer composition from 1% buffer B to 28% B over 45 min, then from 28% buffer B to 40% buffer B over 10 min, and then from 40% buffer B to 100% buffer B over 2 min. The composition was held at 100% buffer B for 3 min and then dropped to 3% buffer B over 5 min and held at 3% buffer B for another 10 min. The Lumos™ mass spectrometer was operated in a data-dependent mode automatically switching between acquisition of a single Orbitrap MS scan (120,000 resolution) every 3 s and MS-MS scan. For each ion selected for fragmentation, Orbitrap HCD (maximum fill time, 100 ms; automatic gain control (AGC) 2×10^5 with a resolution of 30,000), Orbitrap EThcD (maximum fill time, 100 ms; AGC 5×10^4 with a resolution of 30,000), and ion trap collision-induced dissociation (for each selected precursor; maximum fill time, 100 ms; AGC 2×10^4) was performed. The Q-exactive™ HF mass spectrometer was operated in a data-dependent mode automatically switching between acquisition of a single Orbitrap MS scan (120,000 resolution) and 20 MS-MS scans (Orbitrap HCD; maximum fill time, 100 ms; AGC 2×10^5).

Digestion of complex protein lysates for quantitative proteome

Parasites obtained from four T150 flasks confluent with HFFs were purified by filtration and collected by centrifugation (1000 × *g*, 10 min). The parasite pellet was washed three times on ice with ice-cold PBS (2 ml). Parasites were lysed in ice-cold guanidine hydrochloride lysis buffer (6 M GdnHCl, 100 mM Tris (pH 8.5), 10 mM tris(2-carboxyethyl)phosphine, and 40 mM 2-chloroacetamide) and boiled at 95 °C for 10 min with shaking at 2000 rpm to shear DNA and inactivate protease activity, according to the protocol of Humphrey *et al.* (54). Lysates were then cooled for 10 min on ice and then boiled again at 95 °C for 10 min with shaking at 2000 rpm. Lysates were cooled, and protein concentration was determined using a BCA assay. 100 μg of protein from each sample was acetone-precipitated by mixing 4 volumes of ice-cold acetone with 1 volume of sample. Samples were precipitated overnight at −20 °C and then spun down at 4000 × *g* for 10 min at 4 °C. The precipitated protein pellets were resuspended with 80% ice-cold acetone and precipitated for an additional 4 h at −20 °C. Samples were spun down at 17,000 × *g* for 10 min at 4 °C to collect precipitated protein, the supernatant was discarded, and excess acetone was driven off at 65 °C for 5 min. Dried protein pellets were resuspended in 6 M urea, 2 M thiourea, 40 mM NH_4HCO_3, and reduced/alkylated prior to digestion with Lys-C (1/200 w/w) and then trypsin

(1/50 w/w) overnight, as described previously (55). Digested samples were acidified to a final concentration of 0.5% formic acid and desalted using C18 stage tips (53) before analysis by LC-MS.

Quantitative proteome of Δ*tgpofut2* and parental lines using reverse-phase LC-MS

Purified peptides were resuspend in buffer A and separated using a two-column chromatography setup composed of a PepMap100 C18 20 mm × 75 μm trap and a PepMap C18 500 mm × 75 μm analytical column (Thermo Fisher Scientific). Samples were concentrated onto the trap column at 5 μl/min for 5 min and infused into an Orbitrap Fusion™ Lumos™ Tribrid™ mass spectrometer (Thermo Fisher Scientific) at 300 nl/min via the analytical column using a Dionex Ultimate 3000 UPLC (Thermo Fisher Scientific). 180-min gradients were run, altering the buffer composition from 1% buffer B to 28% buffer B over 150 min, then from 28% buffer B to 40% buffer B over 10 min, and then from 40% buffer B to 100% buffer B over 2 min. The composition was held at 100% buffer B for 3 min and then dropped to 3% buffer B over 5 min and held at 3% buffer B for another 10 min. The Lumos™ mass spectrometer was operated in a data-dependent mode automatically switching between the acquisition of a single Orbitrap MS scan (120,000 resolution) every 3 s and MS-MS scans (Orbitrap HCD; maximum fill time, 60 ms; AGC 2×10^5 with a resolution of 15,000).

Mass spectrometry data analysis

Identification of modification events within MIC2 and LFQ analysis was accomplished using MaxQuant (v1.5.3.1) (56). For characterization of MIC2, searches were performed against the *T. gondii* (strain ATCC 50853/GT1) proteome (Uniprot proteome ID UP000005641, downloaded February 4, 2017; 8,450 entries). For LFQ analysis, searches were performed against the *T. gondii* (strain ATCC 50853/GT1) proteome as well as the human (Uniprot proteome ID UP000005640; *H. sapiens*, downloaded October 24, 2013; 84,843 entries). For MIC2 searches, carbamidomethylation of cysteine was set as a fixed modification and the variable modifications of oxidation of methionine, *C*-glycosylation (+162.05 Da to W, allowing the loss of 120 Da because of the characteristic cross-ring fragmentation of the *C*-glycoside), and *O*-fucosylation (+308.11 Da to Ser or Thr, allowing a neutral loss of 308.11). For LFQ searches, carbamidomethylation of cysteine was set as a fixed modification and the variable modifications of oxidation of methionine and acetylation of protein N termini. Searches were performed with semitrypsin cleavage specificity for MIC2 analysis and trypsin cleavage specificity, allowing two miscleavage events for LFQ experiments with a maximum false discovery rate of 1.0% set for protein and peptide identifications. To enhance the identification of peptides between samples, the Match Between Runs option was enabled, with a precursor match window set to 2 min and an alignment window of 10 min. For label-free quantitation, the MaxLFQ option within Maxquant (27) was enabled in addition to the requantification module. The resulting protein group output was processed within the Perseus (v1.4.0.6) (57) analysis environment to remove prior reverse matches and common protein contaminates. For LFQ comparisons, missing values were imputed using Perseus and Pearson correlations visualized using R. All MS proteomics data were deposited in the ProteomeXchange Consortium via the PRIDE (58) partner repository with the dataset identifiers PXD010714 and PXD011440.

Quantitative Western blotting

Parasite samples were lysed for 30 min at 4 °C in 1% (v/v) Triton X-100 and 1 mM $MgCl_2$ in PBS (Gibco), supplemented with final 1× cOmplete protease inhibitors (Sigma) and 0.2% (v/v) benzonase (Merck). Cleared samples were then mixed with an equivalent volume of 2× sample buffer and run on gradient gels. Proteins were then transferred to nitrocellulose and blocked with 5% (w/v) skim milk. Primary and secondary antibodies were diluted in milk/PBS solution. Membranes were probed with mouse anti-MIC2 6D10 and rabbit anti-GAP45 (52) and immunodecorated with LI-COR IRDye 800CW– and IRDye 680RD– conjugated secondary antibodies. Quantitation of the signal proceeded using ImageJ and normalizing the MIC2 signal against GAP45 as a loading control.

Immunofluorescence assay

IFA analysis was performed as described here and elsewhere (59). Briefly, tachyzoite-infected HFFs were fixed with 4% formaldehyde, permeabilized with 0.1% Triton X-100 (v/v), and blocked in 3% BSA/PBS (w/v). Primary and secondary antibodies were added sequentially, washing with PBS in between. Secondary antibodies were conjugated with Alexa Fluor 488 and 594 (Invitrogen). Samples were then imaged on an AP DeltaVision Elite microscope equipped with a CoolSnap2 charge-coupled device (CCD) detector and captured with SoftWorx software (GE Healthcare). Samples were then processed in ImageJ and assembled in Adobe Photoshop.

Invasion assay

The invasion assay proceeded as described previously (60). Briefly, parasites were resuspended in a high [K^+] buffer (142 mM) to suppress motility, added to host cells, and allowed to settle. The buffer was then exchanged with DME supplemented with 1% fetal bovine serum, and parasites were allowed to invade for 2, 10, and 30 min at 37 °C. Then they were chemically fixed in 2.5% formaldehyde and 0.02% glutaraldehyde for 10 min each. The wells were then washed three times with PBS (pH 7.4) and were blocked with 3% BSA in PBS (pH 7.4) overnight at 4 °C. IFA proceeded as standard using antibodies against SAG1 to detect extracellular parasites and then permeabilization with 0.1% Triton X-100. GAP45 antibodies were then used to mark all parasites. The invasion rate was determined by counting the number of $SAG1^+$ parasites compared with total ($GAP45^+$).

Plaque assay

Plaque assays were carried out by inoculating 120 parasites into each well of a 6-well plate in D1 medium and allowed to grow undisturbed for 7–8 days. Cultures were fixed in 4% paraformaldehyde and incubated for 1 h at room temperature. Host cells were then stained using 2% crystal violet and washed.

Author contributions—S. K., M. J. C., A. J., A. D. U., R. J. S., and N. E. S. investigation; S. K., M. J. C., A. J., A. D. U., R. J. S., and N. E. S. methodology; S. K., M. J. C., A. J., A. D. U., M.-H. H., R. J. S., V. C., C. J. T., E. D. G.-B., and N. E. S. writing-review and editing; V. C. and N. E. S. resources; C. J. T. and E. D. G.-B. conceptualization; C. J. T. and E. D. G.-B. supervision; C. J. T., E. D. G.-B., and N. E. S. funding acquisition; E. D. G.-B. project administration; N. E. S. visualization; N. E. S. writing-original draft.

Acknowledgments—We thank L. David Sibley for the kind gift of the pCas9-GFP plasmid and anti-MIC2 mAb 6D10 as well as Giel Van Dooren for the kind gift of the pgCH plasmid. We would also like to thank the Melbourne Mass Spectrometry and Proteomics Facility of The Bio21 Molecular Science and Biotechnology Institute at The University of Melbourne for support, maintenance, and access to MS infrastructure. We are also grateful for institutional support from the Victorian State Government Operational Infrastructure Support and the Australian Government NHMRC Independent Research Institute Infrastructure Support Scheme (IRIISS).

Note added in proof—Fig. 1 contained an inadvertently duplicated image in the version of this article published as a Paper in Press on December 4, 2018. This error has now been corrected and does not affect the results or conclusions of this work.

References

1. Furtado, J. M., Smith, J. R., Belfort, R., Jr., Gattey, D., and Winthrop, K. L. (2011) Toxoplasmosis: a global threat. *J. Glob. Infect. Dis.* **3,** 281–284 CrossRef Medline
2. Montoya, J. G., and Liesenfeld, O. (2004) Toxoplasmosis. *Lancet* **363,** 1965–1976 CrossRef Medline
3. Jones, J., Lopez, A., and Wilson, M. (2003) Congenital toxoplasmosis. *Am. Fam. Physician* **67,** 2131–2138 Medline
4. Frénal, K., Dubremetz, J. F., Lebrun, M., and Soldati-Favre, D. (2017) Gliding motility powers invasion and egress in Apicomplexa. *Nat. Rev. Microbiol.* **15,** 645–660 CrossRef Medline
5. Carruthers, V. B., Giddings, O. K., and Sibley, L. D. (1999) Secretion of micronemal proteins is associated with *toxoplasma* invasion of host cells. *Cell. Microbiol.* **1,** 225–235 CrossRef Medline
6. Boucher, L. E., and Bosch, J. (2015) The apicomplexan glideosome and adhesins: structures and function. *J. Struct. Biol.* **190,** 93–114 CrossRef Medline
7. Tardieux, I., and Baum, J. (2016) Reassessing the mechanics of parasite motility and host-cell invasion. *J. Cell Biol.* **214,** 507–515 CrossRef Medline
8. Horuk, R., Chitnis, C. E., Darbonne, W. C., Colby, T. J., Rybicki, A., Hadley, T. J., and Miller, L. H. (1993) A receptor for the malarial parasite *Plasmodium vivax*: the erythrocyte chemokine receptor. *Science* **261,** 1182–1184 CrossRef Medline
9. Cowman, A. F., Tonkin, C. J., Tham, W. H., and Duraisingh, M. T. (2017) The molecular basis of erythrocyte invasion by malaria parasites. *Cell Host Microbe* **22,** 232–245 CrossRef Medline
10. Huynh, M. H., and Carruthers, V. B. (2006) *Toxoplasma* MIC2 is a major determinant of invasion and virulence. *PLoS Pathog.* **2,** e84 CrossRef Medline
11. Hofsteenge, J., Huwiler, K. G., Macek, B., Hess, D., Lawler, J., Mosher, D. F., and Peter-Katalinic, J. (2001) *C*-mannosylation and *O*-fucosylation of the thrombospondin type 1 module. *J. Biol. Chem.* **276,** 6485–6498 CrossRef Medline
12. Ricketts, L. M., Dlugosz, M., Luther, K. B., Haltiwanger, R. S., and Majerus, E. M. (2007) *O*-fucosylation is required for ADAMTS13 secretion. *J. Biol. Chem.* **282,** 17014–17023 CrossRef Medline
13. Wang, L. W., Dlugosz, M., Somerville, R. P., Raed, M., Haltiwanger, R. S., and Apte, S. S. (2007) *O*-fucosylation of thrombospondin type 1 repeats in ADAMTS-like-1/punctin-1 regulates secretion: implications for the ADAMTS superfamily. *J. Biol. Chem.* **282,** 17024–17031 CrossRef Medline
14. Benz, B. A., Nandadasa, S., Takeuchi, M., Grady, R. C., Takeuchi, H., LoPilato, R. K., Kakuda, S., Somerville, R. P. T., Apte, S. S., Haltiwanger, R. S., and Holdener, B. C. (2016) Genetic and biochemical evidence that gastrulation defects in Pofut2 mutants result from defects in ADAMTS9 secretion. *Dev. Biol.* **416,** 111–122 CrossRef Medline
15. Du, J., Takeuchi, H., Leonhard-Melief, C., Shroyer, K. R., Dlugosz, M., Haltiwanger, R. S., and Holdener, B. C. (2010) *O*-fucosylation of thrombospondin type 1 repeats restricts epithelial to mesenchymal transition (EMT) and maintains epiblast pluripotency during mouse gastrulation. *Dev. Biol.* **346,** 25–38 CrossRef Medline
16. Niwa, Y., Suzuki, T., Dohmae, N., and Simizu, S. (2015) *O*-Fucosylation of CCN1 is required for its secretion. *FEBS Lett.* **589,** 3287–3293 CrossRef Medline
17. Swearingen, K. E., Lindner, S. E., Flannery, E. L., Vaughan, A. M., Morrison, R. D., Patrapuvich, R., Koepfli, C., Muller, I., Jex, A., Moritz, R. L., Kappe, S. H. I., Sattabongkot, J., and Mikolajczak, S. A. (2017) Proteogenomic analysis of the total and surface-exposed proteomes of *Plasmodium vivax* salivary gland sporozoites. *PLoS Negl. Trop. Dis.* **11,** e0005791 CrossRef Medline
18. Swearingen, K. E., Lindner, S. E., Shi, L., Shears, M. J., Harupa, A., Hopp, C. S., Vaughan, A. M., Springer, T. A., Moritz, R. L., Kappe, S. H., and Sinnis, P. (2016) Interrogating the *Plasmodium* sporozoite surface: identification of surface-exposed proteins and demonstration of glycosylation on CSP and TRAP by mass spectrometry-based proteomics. *PLoS Pathog.* **12,** e1005606 CrossRef Medline
19. Lopaticki, S., Yang, A. S. P., John, A., Scott, N. E., Lingford, J. P., O'Neill, M. T., Erickson, S. M., McKenzie, N. C., Jennison, C., Whitehead, L. W., Douglas, D. N., Kneteman, N. M., Goddard-Borger, E. D., and Boddey, J. A. (2017) Protein *O*-fucosylation in *Plasmodium falciparum* ensures efficient infection of mosquito and vertebrate hosts. *Nat. Commun.* **8,** 561 CrossRef Medline
20. Goddard-Borger, E. D., and Boddey, J. A. (2018) Implications of *Plasmodium* glycosylation on vaccine efficacy and design. *Future Microbiol.* **13,** 609–612 CrossRef Medline
21. Hoppe, C. M., Albuquerque-Wendt, A., Bandini, G., Leon, D. R., Shcherbakova, A., Buettner, F. F. R., Izquierdo, L., Costello, C. E., Bakker, H., and Routier, F. H. (2018) Apicomplexan C-mannosyltransferases modify thrombospondin type I-containing adhesins of the TRAP family. *Glycobiology* **28,** 333–343 Medline
22. Frese, C. K., Altelaar, A. F., van den Toorn, H., Nolting, D., Griep-Raming, J., Heck, A. J., and Mohammed, S. (2012) Toward full peptide sequence coverage by dual fragmentation combining electron-transfer and higher-energy collision dissociation tandem mass spectrometry. *Anal. Chem.* **84,** 9668–9673 CrossRef Medline
23. Hartmann, S., and Hofsteenge, J. (2000) Properdin, the positive regulator of complement, is highly C-mannosylated. *J. Biol. Chem.* **275,** 28569–28574 CrossRef Medline
24. Chen, C. I., Keusch, J. J., Klein, D., Hess, D., Hofsteenge, J., and Gut, H. (2012) Structure of human POFUT2: insights into thrombospondin type 1 repeat fold and *O*-fucosylation. *EMBO J.* **31,** 3183–3197 CrossRef Medline
25. Nothaft, H., and Szymanski, C. M. (2013) Bacterial protein *N*-glycosylation: new perspectives and applications. *J. Biol. Chem.* **288,** 6912–6920 CrossRef Medline
26. Yang, X., and Qian, K. (2017) Protein *O*-GlcNAcylation: emerging mechanisms and functions. *Nat. Rev. Mol. Cell Biol.* **18,** 452–465 CrossRef Medline
27. Cox, J., Hein, M. Y., Luber, C. A., Paron, I., Nagaraj, N., and Mann, M. (2014) Accurate proteome-wide label-free quantification by delayed normalization and maximal peptide ratio extraction, termed MaxLFQ. *Mol. Cell. Proteomics* **13,** 2513–2526 CrossRef Medline
28. Andenmatten, N., Egarter, S., Jackson, A. J., Jullien, N., Herman, J. P., and Meissner, M. (2013) Conditional genome engineering in *Toxoplasma gondii* uncovers alternative invasion mechanisms. *Nat. Methods* **10,** 125–127 CrossRef Medline
29. Whitelaw, J. A., Latorre-Barragan, F., Gras, S., Pall, G. S., Leung, J. M., Heaslip, A., Egarter, S., Andenmatten, N., Nelson, S. R., Warshaw, D. M.,

Ward, G. E., and Meissner, M. (2017) Surface attachment, promoted by the actomyosin system of *Toxoplasma gondii* is important for efficient gliding motility and invasion. *BMC Biol.* **15,** 1 CrossRef Medline

30. Gras, S., Jackson, A., Woods, S., Pall, G., Whitelaw, J., Leung, J. M., Ward, G. E., Roberts, C. W., and Meissner, M. (2017) Parasites lacking the micronemal protein MIC2 are deficient in surface attachment and host cell egress, but remain virulent *in vivo*. *Wellcome Open Res.* **2,** 32 CrossRef Medline
31. Pinger, J., Nešić, D., Ali, L., Aresta-Branco, F., Lilic, M., Chowdhury, S., Kim, H. S., Verdi, J., Raper, J., Ferguson, M. A. J., Papavasiliou, F. N., and Stebbins, C. E. (2018) African trypanosomes evade immune clearance by *O*-glycosylation of the VSG surface coat. *Nat. Microbiol.* **3,** 932–938 CrossRef Medline
32. Valero-González, J., Leonhard-Melief, C., Lira-Navarrete, E., Jiménez-Osés, G., Hernández-Ruiz, C., Pallarés, M. C., Yruela, I., Vasudevan, D., Lostao, A., Corzana, F., Takeuchi, H., Haltiwanger, R. S., and Hurtado-Guerrero, R. (2016) A proactive role of water molecules in acceptor recognition by protein *O*-fucosyltransferase 2. *Nat. Chem. Biol.* **12,** 240–246 CrossRef Medline
33. Kozma, K., Keusch, J. J., Hegemann, B., Luther, K. B., Klein, D., Hess, D., Haltiwanger, R. S., and Hofsteenge, J. (2006) Identification and characterization of a β1,3-glucosyltransferase that synthesizes the Glc-β1,3-Fuc disaccharide on thrombospondin type 1 repeats. *J. Biol. Chem.* **281,** 36742–36751 CrossRef Medline
34. Sato, T., Sato, M., Kiyohara, K., Sogabe, M., Shikanai, T., Kikuchi, N., Togayachi, A., Ishida, H., Ito, H., Kameyama, A., Gotoh, M., and Narimatsu, H. (2006) Molecular cloning and characterization of a novel human β1,3-glucosyltransferase, which is localized at the endoplasmic reticulum and glucosylates *O*-linked fucosylglycan on thrombospondin type 1 repeat domain. *Glycobiology* **16,** 1194–1206 CrossRef Medline
35. Lesnik Oberstein, S. A., Kriek, M., White, S. J., Kalf, M. E., Szuhai, K., den Dunnen, J. T., Breuning, M. H., and Hennekam, R. C. (2006) Peters Plus syndrome is caused by mutations in B3GALTL, a putative glycosyltransferase. *Am. J. Hum. Genet.* **79,** 562–566 CrossRef Medline
36. Vasudevan, D., Takeuchi, H., Johar, S. S., Majerus, E., and Haltiwanger, R. S. (2015) Peters plus syndrome mutations disrupt a noncanonical ER quality-control mechanism. *Curr. Biol.* **25,** 286–295 CrossRef Medline
37. Vasudevan, D., and Haltiwanger, R. S. (2014) Novel roles for *O*-linked glycans in protein folding. *Glycoconj. J.* **31,** 417–426 CrossRef Medline
38. Sultan, A. A., Thathy, V., Frevert, U., Robson, K. J., Crisanti, A., Nussenzweig, V., Nussenzweig, R. S., and Ménard, R. (1997) TRAP is necessary for gliding motility and infectivity of *Plasmodium* sporozoites. *Cell* **90,** 511–522 CrossRef Medline
39. Sidik, S. M., Huet, D., Ganesan, S. M., Huynh, M. H., Wang, T., Nasamu, A. S., Thiru, P., Saeij, J. P. J., Carruthers, V. B., Niles, J. C., and Lourido, S. (2016) A genome-wide CRISPR screen in *Toxoplasma* identifies essential apicomplexan genes. *Cell* **166,** 1423–1435.e12 CrossRef Medline
40. Marino, N. D., Panas, M. W., Franco, M., Theisen, T. C., Naor, A., Rastogi, S., Buchholz, K. R., Lorenzi, H. A., and Boothroyd, J. C. (2018) Identification of a novel protein complex essential for effector translocation across the parasitophorous vacuole membrane of *Toxoplasma gondii*. *PLoS Pathog.* **14,** e1006828 CrossRef Medline
41. Jung, C., Lee, C. Y., and Grigg, M. E. (2004) The SRS superfamily of *Toxoplasma* surface proteins. *Int. J. Parasitol.* **34,** 285–296 CrossRef Medline
42. Wasmuth, J. D., Pszenny, V., Haile, S., Jansen, E. M., Gast, A. T., Sher, A., Boyle, J. P., Boulanger, M. J., Parkinson, J., and Grigg, M. E. (2012) Integrated bioinformatic and targeted deletion analyses of the SRS gene superfamily identify SRS29C as a negative regulator of *Toxoplasma* virulence. *MBio* **3,** e00321–12 Medline
43. Huynh, M. H., Liu, B., Henry, M., Liew, L., Matthews, S. J., and Carruthers, V. B. (2015) Structural basis of *Toxoplasma gondii* MIC2-associated protein interaction with MIC2. *J. Biol. Chem.* **290,** 1432–1441 CrossRef Medline
44. Huynh, M. H., Rabenau, K. E., Harper, J. M., Beatty, W. L., Sibley, L. D., and Carruthers, V. B. (2003) Rapid invasion of host cells by *Toxoplasma* requires secretion of the MIC2-M2AP adhesive protein complex. *EMBO J.* **22,** 2082–2090 CrossRef Medline
45. Rabenau, K. E., Sohrabi, A., Tripathy, A., Reitter, C., Ajioka, J. W., Tomley, F. M., and Carruthers, V. B. (2001) TgM2AP participates in *Toxoplasma gondii* invasion of host cells and is tightly associated with the adhesive protein TgMIC2. *Mol. Microbiol.* **41,** 537–547 CrossRef Medline
46. Huynh, M. H., Opitz, C., Kwok, L. Y., Tomley, F. M., Carruthers, V. B., and Soldati, D. (2004) Trans-genera reconstitution and complementation of an adhesion complex in *Toxoplasma gondii*. *Cell. Microbiol.* **6,** 771–782 CrossRef Medline
47. Moudy, R., Manning, T. J., and Beckers, C. J. (2001) The loss of cytoplasmic potassium upon host cell breakdown triggers egress of *Toxoplasma gondii*. *J. Biol. Chem.* **276,** 41492–41501 CrossRef Medline
48. Uboldi, A. D., Wilde, M. L., McRae, E. A., Stewart, R. J., Dagley, L. F., Yang, L., Katris, N. J., Hapuarachchi, S. V., Coffey, M. J., Lehane, A. M., Botte, C. Y., Waller, R. F., Webb, A. I., McConville, M. J., and Tonkin, C. J. (2018) Protein kinase A negatively regulates Ca^{2+} signalling in *Toxoplasma gondii*. *PLoS Biol.* **16,** e2005642 CrossRef Medline
49. Huynh, M. H., and Carruthers, V. B. (2009) Tagging of endogenous genes in a *Toxoplasma gondii* strain lacking Ku80. *Eukaryot. Cell* **8,** 530–539 CrossRef Medline
50. Shen, B., Brown, K. M., Lee, T. D., and Sibley, L. D. (2014) Efficient gene disruption in diverse strains of *Toxoplasma gondii* using CRISPR/CAS9. *MBio* **5,** e01114–e01114 Medline
51. Long, S., Wang, Q., and Sibley, L. D. (2016) Analysis of noncanonical calcium-dependent protein kinases in *Toxoplasma gondii* by targeted gene deletion using CRISPR/Cas9. *Infect. Immun.* **84,** 1262–1273 CrossRef Medline
52. Kang, D., Gho, Y. S., Suh, M., and Kang, C. (2002) Highly sensitive and fast protein detection with Coomassie Brilliant Blue in sodium dodecyl sulfate-polyacrylamide gel electrophoresis. *Bull. Korean Chem. Soc.* **23,** 2
53. Rappsilber, J., Mann, M., and Ishihama, Y. (2007) Protocol for micro-purification, enrichment, pre-fractionation and storage of peptides for proteomics using StageTips. *Nat. Protoc.* **2,** 1896–1906 CrossRef Medline
54. Humphrey, S. J., Azimifar, S. B., and Mann, M. (2015) High-throughput phosphoproteomics reveals *in vivo* insulin signaling dynamics. *Nat. Biotechnol.* **33,** 990–995 CrossRef Medline
55. Scott, N. E., Parker, B. L., Connolly, A. M., Paulech, J., Edwards, A. V., Crossett, B., Falconer, L., Kolarich, D., Djordjevic, S. P., Højrup, P., Packer, N. H., Larsen, M. R., and Cordwell, S. J. (2011) Simultaneous glycan-peptide characterization using hydrophilic interaction chromatography and parallel fragmentation by CID, higher energy collisional dissociation, and electron transfer dissociation MS applied to the *N*-linked glycoproteome of *Campylobacter jejuni*. *Mol. Cell. Proteomics* **10,** M000031-MCP201 Medline
56. Cox, J., and Mann, M. (2008) MaxQuant enables high peptide identification rates, individualized p.p.b.-range mass accuracies and proteome-wide protein quantification. *Nat. Biotechnol.* **26,** 1367–1372 CrossRef Medline
57. Tyanova, S., Temu, T., Carlson, A., Sinitcyn, P., Mann, M., and Cox, J. (2015) Visualization of LC-MS/MS proteomics data in MaxQuant. *Proteomics* **15,** 1453–1456 CrossRef Medline
58. Vizcaíno, J. A., Csordas, A., del-Toro, N., Dianes, J. A., Griss, J., Lavidas, I., Mayer, G., Perez-Riverol, Y., Reisinger, F., Ternent, T., Xu, Q. W., Wang, R., and Hermjakob, H. (2016) 2016 update of the PRIDE database and its related tools. *Nucleic Acids Res.* **44,** D447–D456 CrossRef Medline
59. Coffey, M. J., Dagley, L. F., Seizova, S., Kapp, E. A., Infusini, G., Roos, D. S., Boddey, J. A., Webb, A. I., and Tonkin, C. J. (2018) Aspartyl protease 5 matures dense granule proteins that reside at the host-parasite interface in *Toxoplasma gondii*. *MBio* **9,** e01796-18 Medline
60. Kafsack, B. F., Beckers, C., and Carruthers, V. B. (2004) Synchronous invasion of host cells by *Toxoplasma gondii*. *Mol. Biochem. Parasitol.* **136,** 309–311 CrossRef Medline
61. Peng, D., and Tarleton, R. (2015) EuPaGDT: A web tool tailored to design CRISPR guide RNAs for eukaryotic pathogens. *Microb. Genom.* **1,** e000033 CrossRef Medline
62. Bandini, G., Leon, D. R., Hoppe, C. M., Zhang, Y., Agop-Nersesian, C., Shears, M. J., Mahal, L. K, Routier, F. H., Costello, C. E., and Samuelson, J. (2019) *O*-Fucosylation of thrombospondin-like repeats is required for processing of microneme protein 2 and for efficient host cell invasion by *Toxoplasma gondii* tachyzoites. *J. Biol. Chem.* **294,** 1967–1983 CrossRef Medline